Improved ocean circulation modeling with combined effects of surface waves and M2 internal tides on vertical mixing: a case study for the Indian Ocean

Zhanpeng Zhuang[1, 2, 3], Quanan Zheng [4], Yongzeng Yang[1,2,3], Zhenya Song[1,2,3], Yeli Yuan[1,2,3], Chaojie Zhou[5], Xinhua Zhao[6], Ting Zhang[1], Jing Xie[7]

[1]First Institute of Oceanography, and Key Laboratory of Marine Science and Numerical Modeling, Ministry of Natural Resources, Qingdao 266061, China

[2]Laboratory for Regional Oceanography and Numerical Modeling, Pilot National Laboratory for Marine Science and Technology, Qingdao 266237, China

[3]Shandong Key Laboratory of Marine Science and Numerical Modeling, Qingdao 266061, China

[4]Department of Atmospheric and Oceanic Science, University of Maryland, College Park, Maryland 20740-20742, USA

[5]Hainan Institute of Zhejiang University, Yazhou Bay Science and Technology City, Sanya 572025, China

[6]Jiangsu Marine Resources Development Research Institute, Jiangsu Ocean University, Lianyungang 222005, China

[7]School of Information and Control Engineering, Qingdao University of Technology, Qingdao 266520, China

Correspondence to: Zhanpeng Zhuang (zhuangzp@fio.org.cn)

Abstract. The surface waves and internal tides have great contribution to the vertical mixing processes in the upper ocean. In this study, three mixing schemes, including the non-breaking surface-wave-generated turbulent mixing, the mixing induced by the wave transport flux residue, and the internal-tide-generated turbulent mixing, are introduced to study the effects the surface waves and the internal tides on the vertical mixing. The three schemes are jointly incorporated into the Marine Science and Numerical Modeling (MASNUM) ocean circulation model as a part of the vertical diffusive terms, which are calculated by the surface wave parameters simulated from the MASNUM wave model and the surface amplitudes of the mode-1 M_2 internal tides extracted from the satellite altimetry data using a two-dimensional plane wave fit method. The effects of the mixing schemes on the Indian Ocean modeling are tested by five climatological experiments. The surface waves and internal tides lead to enhance the vertical mixing processes in the sea surface and ocean interior, respectively. The combination of the mixing schemes is able to strengthen the vertical water exchange and draw more water from the sea surface to the ocean interior. The simulated results gain significant improvement in the thermal structure and the mixed layer depth if the three schemes are all adopted.

1 Introduction

30

Turbulence in the ocean is hard to be described superficially and characterized dynamically. Fortunately, in recent years a great progress in understanding the turbulence has been achieved by a combination of experiments, simulations, and theories (Baumert et al., 2005; Umlauf and Burchard, 2020). Turbulence has great contribution to the vertical mixing processes in the upper ocean, which is important for regulating the sea surface temperature (SST) and the thermal structure. Accurate

35 parameterization of the vertical mixing process is the key for the ocean general circulation models (OGCMs) to simulate the realistic ocean dynamic and thermal environment. However, the factors influencing the vertical mixing in the upper ocean still remain unclearly, so that there are substantial biases in the simulated SST, mixed layer depth (MLD) and dynamic quantities within the ocean interior such as potential vorticity, temperature and salinity for the most ocean models (Ezer, 2000; Qiao et al., 2010; Song et al., 2020; Wang et al., 2019; Zhuang et al., 2020).

40

In the sea surface layer, turbulence can be generated by wind and surface waves (Agrawal et al., 1992; Babanin, 2017; Qiao et al., 2004), Langmuir circulation (Li and Garrett, 1997; Li and Fox-Kemper, 2017; Yu et al., 2018), and surface cooling at night (Shay and Gregg, 1986). Among them wind energy input to the surface waves is estimated as 60 - 70 TW (Wang and Huang, 2004) much greater than all other mechanical energy sources (Wunsch and Ferrari, 2004). Most of the wave energy is dissipated locally through wave breaking (Donelan, 1998), and enhances the turbulent mixing near the sea surface. Meanwhile,

45 previous studies indicated that the non-breaking surface waves enable to affect the depths much greater than that of wave breaking (Huang et al., 2011), and even penetrate into the sub-thermocline ocean (Babanin and Haus, 2009; Wang et al., 2019). Despite the parameterization schemes of the wave-induced mixing have been developed and adopted in OGCMs, it still remains controversial about the effects of wave-induced turbulence mixing in the upper ocean (Huang and Qiao, 2010; Kantha et al., 2014).

50

In the bulk of the stratified ocean interior, it is believed that the internal waves are one of the dominant sources to induce turbulent mixing (Munk and Wunsch, 1998; Wunsch and Ferrari, 2004). The total internal wave energy input was estimated as 2.1 ± 0.7 TW (Kunze, 2017) with most of the uncertainty in the observations of the near-inertial waves produced by winds (Alford, 2001; Furuichi et al., 2008) and the internal lee-waves (Scott et al., 2011; Wright et al., 2014). Based on the internal wave-wave interaction theory, parameterization schemes for internal-wave-induced turbulence mixing are proposed in terms

55 of shear and/or strain (e.g. Gregg and Kunze, 1991; Gregg et al., 2003; Huussen et al., 2012; Kunze et al., 2006). However, the usefulness of the parameterizations, which are put forward based on particular data set, should be severely limited (Polzin et al., 2014). The development of the dynamical interpretation and parameterization of the internal-wave-induced turbulence mixing is still an ongoing process. Meanwhile, the internal tides are essentially the internal waves generated by barotropic tidal flow with the tidal frequency. Previous investigators have demonstrated that the internal tides are important and even dominant

60 in the energy budgets of the ocean interior (Wunsch and Ferrari, 2004; Zhao et al., 2016). In this study, we analyze the effects of the turbulent mixing generated by the M_2 internal tides on the ocean circulation. The internal tides are extracted from the satellite altimeter data using a two-dimensional plane wave fit method (Zhao, 2018; Zhao et al., 2016).

The Indian Ocean (IO) is the third largest ocean in the world and has an important low latitude connection to the Pacific Ocean through the Indonesian Archipelago (Fig. 1). On one hand, the mean wind pattern of the South Indian Ocean (SIO) is

65   similar to the Atlantic and Pacific Oceans, with westerly winds at high latitude (Southern Ocean) and trade winds at low latitudes; on the other hand, a complex annual cycle associated with the seasonally reversing monsoons is dominant in the North Indian Ocean (NIO). As a result, the wind waves, which are the prominent feature of the ocean surface, undergo large seasonal variations in the NIO (Kumar et al., 2013; Kumar et al., 2018). Previous investigations showed that the annual and seasonal (during summer monsoon period, i.e. June - September) average significant wave height (SWH) in the NIO ranges

70   from 1.5 - 2.5 m and 3.0 - 3.5 m, respectively, based on the European Centre for Medium-Range Weather Forecasts (ECMWF) ReAnalysis V5 (ERA5) reanalysis product (Anoop et al., 2015). In the SIO, the average SWH between 35° S and 22° S is consistently higher by about 1.5 times that in the NIO because of the higher wind speed (Kumar et al., 2013). Furthermore, based on the satellite altimetry data and high-resolution numerical simulations, a regional map of the internal tides in the IO was constructed by previous studies. The results show that the Madagascar-Mascarene regions, the Bay of Bengal and the

75   Andaman Sea are considered to be hot spots for generation of semidiurnal internal tides (Ansong et al., 2017; Zhao, 2018), while the central IO for diurnal internal tides (Shriver et al., 2012). In summary, all these efforts gave us a strong hint that the surface waves and the internal tides in the IO could not be neglected in the studies of ocean dynamics and modeling.
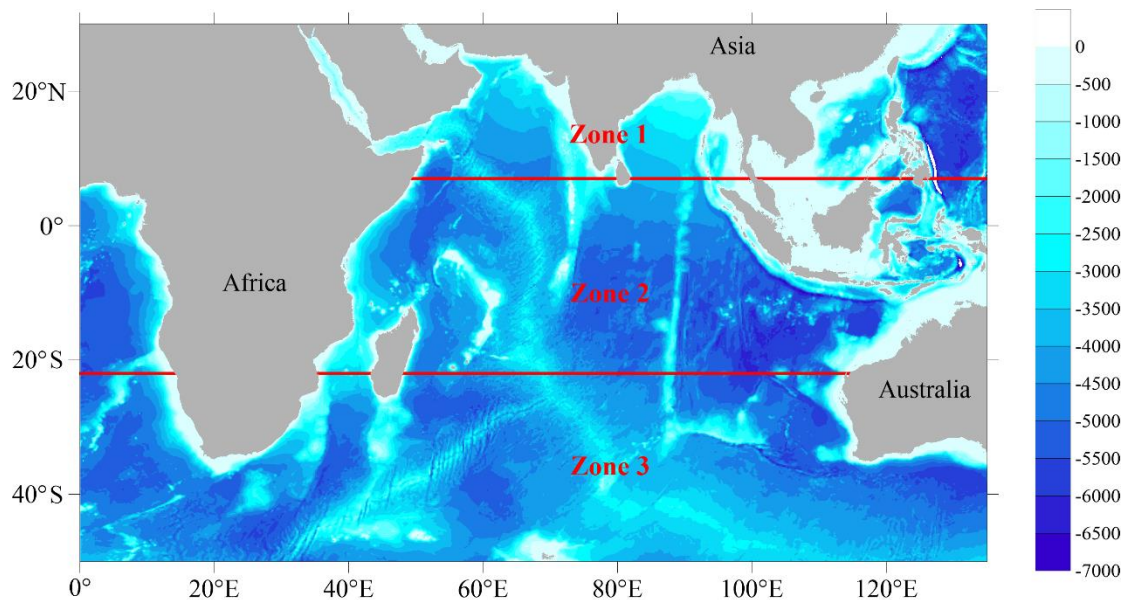
Figure 1: Bathymetric map (color codes in m) in the Indian Ocean. Red lines (7° N and 22° S) show the zone partition in the present
80   **study**

In this study, the vertical mixing schemes induced by non-breaking surface waves and internal tides are incorporated into the MASNUM ocean circulation model (Han, 2014; Han and Yuan, 2014; Zhuang et al., 2018). The vertical mixing schemes are introduced in Section 2. Section 3 describes the model and experiment design. Model results are given in Section 4. The relevant discussion is given in Section 5 and the conclusions are summarized in Section 6.

2 Vertical Mixing Schemes

2.1 Non-breaking Surface-wave-generated Turbulent Mixing

Previous studies indicated that the non-breaking surface waves are able to enhance the turbulent mixing in the upper ocean (Babanin and Haus, 2009; Dai et al., 2010; Huang and Qiao, 2010; Qiao et al., 2016). The ability to simulate the SST and the MLD can be improved obviously via the incorporation of the related non-breaking wave-induced turbulent mixing schemes into the OGCMs (Aijaz et al., 2017; Lin et al., 2006; Song et al., 2007; Wang et al., 2019; Xia et al., 2006). According to Yuan et al. (2011) and Yuan et al. (2013), Zhuang et al. (2020) expressed the vertical viscosity, B_{us}, and diffusivity, B_{Ts}, generated by the non-breaking surface waves (NBSW) as follows,

$$
\begin{cases}
B_{us} = \left(\frac{7}{4}\right)^{1/2} \cdot h_{sw}^2 \cdot \left(\sum_{i=1}^{3}\sum_{j=1}^{3}\left|\frac{\partial u_i}{\partial x_j}\right|\right)_{sw}^2 \bigg/ \left(\sum_{i=1}^{3}\sum_{j=1}^{3}\left|\frac{\partial u_i}{\partial x_j}\right|_{x_3=0}\right)_{sw} \\
B_{Ts} = \frac{1}{\sigma}\left(\frac{7}{4}\right)^{1/2} \cdot h_{sw}^2 \cdot \left(\sum_{i=1}^{3}\sum_{j=1}^{3}\left|\frac{\partial u_i}{\partial x_j}\right|\right)_{sw}^2 \bigg/ \left(\sum_{i=1}^{3}\sum_{j=1}^{3}\left|\frac{\partial u_i}{\partial x_j}\right|_{x_3=0}\right)_{sw}
\end{cases} ,
\tag{1}
$$

where h_{sw} is the significant wave height, $\left(\sum_{i=1}^{3}\sum_{j=1}^{3}\left|\frac{\partial u_i}{\partial x_j}\right|\right)_{sw}$ is the the averaged velocity shear module of the sea surface waves and can be calculated as

$$
\left(\sum_{i=1}^{3}\sum_{j=1}^{3}\left|\frac{\partial u_i}{\partial x_j}\right|\right)_{sw}^2 = 2\iint_{\vec{k}} \Phi_{sw} K_{sw}^2 \omega_{sw}^2 \frac{\cosh\left[2K_{sw}(x_3 - H)\right]}{\sinh^2\left[K_{sw} \cdot (-H)\right]} dk_1 dk_2 ,
\tag{2}
$$

where ω_{sw} is the surface wave frequency in a typical frequency range: $\omega_{sw} > N$, where N denotes the Brunt-Väisälä frequency, K_{sw} is the wave number, H is the water depth. $\Phi_{sw} = \eta_{sw} \cdot \eta_{sw}^*$ is the wave number spectrum of h_{sw}, η_{sw} is the Fourier kernel function of h_{sw}, i.e., $h_{sw} = \iint \eta_{sw} \exp\left\{i\left(k_1 x + k_2 y - \omega t\right)\right\} dk_1 dk_2$, here superscript "*" means the conjugate value, k_1 and k_2 are the horizontal components of the wave number in x- and y- directions.

2.2. Mixing induced by surface wave transport flux residue

Apart from the NBSWs, the residue of the wave transport flux is also able to contribute to inducing the mixing to the ocean circulation through the Reynolds average upon characteristic wavelength scale (Yang et al., 2019; Yang et al., 2009). Yang et al. (2009) proposed a mixing scheme for the wave transport flux residue (WTFR), which has been adopted in the OGCMs (Shi et al., 2016; Yu et al., 2020). The results show that the simulated SST and MLD are remarkably improved especially in summer and in the strong current regions. In the tropical cyclone conditions, the performance of the model to simulate ocean response could also be greatly improved, if the wave transport flux residue mixing scheme is introduced. The coefficients of the wave transport flux residue mixing are expressed as follows,

$$\begin{cases} B_{\text{SM1}} = \iint\limits_{\vec{k}} \omega k_1 E\left(\vec{k}\right) \dfrac{\cosh\left[2K(x_3-H)\right]}{\sinh^2\left[K\cdot(-H)\right]} dk_1 dk_2 \\[4mm] B_{\text{SM2}} = \iint\limits_{\vec{k}} \omega k_2 E\left(\vec{k}\right) \dfrac{\cosh\left[2K(x_3-H)\right]}{\sinh^2\left[K\cdot(-H)\right]} dk_1 dk_2 \end{cases}, \tag{3}$$

110 where $E\left(\vec{k}\right)$ represents the wave number spectrum, which can be calculated from the wave spectrum model, other variables are the same as that in Eq. (2).

2.3. Internal-tide-generated Turbulent Mixing

In the stratified ocean interior, the internal tides (IT) are able to provide about half of the mechanical power required for the ocean interior turbulent mixing (Vic et al., 2019; Whalen et al., 2020; Wunsch and Ferrari, 2004; Zhao, 2018). However,

115 the currently field observations are insufficient for constructing the whole internal-tide map in the IO. Satellite altimetry is able to provide sea surface height (SSH) measurements to observe the global internal tides (Ray and Mitchum, 1996). Zhao et al. (2016) presented a method to extract the M_2 internal tides by fitting plane waves to satellite altimeter data in individual windows with size of 160 km × 160 km. In this technique, the least square fitting algorithm is adopted to determine the amplitude and phase of one plane wave. This procedure can be repeated three times to extract the three most dominant M_2

120 internal waves, of which superposition gives the final internal tidal solution. In this study, the turbulent mixing generated by M_2 semidiurnal internal tides will be derived from the SSH amplitude (Zhao et al., 2016). Other principal tidal constituents will be studied in future. For simplicity, the mode-1 M_2 internal tides, which mainly originate from regions with steep topographic gradients, are considered, because the depth-integrated energy and SSH amplitudes of the mode-2 M_2 internal tides are much smaller than mode-1 ones (Zhao, 2018).

125 Yuan et al. (2013) presented the second-order turbulence closure model to estimate the turbulence kinetic energy and dissipation in terms of the velocity shear module of the non-breaking waves. The sub-surface displacements of internal tides, pressure anomalies and currents can be derived from the SSH amplitudes following vertical models (Wunsch, 2013; Zhao, 2014; Zhao and Alford, 2009). The detailed derivation process about the velocity shear module of the internal tide can be found in Appendix A. For the mode-1 M_2 internal tide, the vertical viscosity, B_{ui}, and diffusivity, B_{Ti}, generated by the velocity

130 shear can be written as follows,

$$\begin{cases} B_{ui} = \left(\dfrac{7}{4}\right)^{1/2} \cdot h_{\text{iw}}^2 \cdot \left. \left(\displaystyle\sum_{i=1}^{3}\sum_{j=1}^{3}\left|\dfrac{\partial u_i}{\partial x_j}\right|\right)^2_{\text{iw}} \middle/ \left(\displaystyle\sum_{i=1}^{3}\sum_{j=1}^{3}\left|\dfrac{\partial u_i}{\partial x_j}\right|_{x_3=0}\right)_{\text{iw}} \right. \\[6mm] B_{Ti} = \dfrac{1}{\sigma}\left(\dfrac{7}{4}\right)^{1/2} \cdot h_{\text{iw}}^2 \cdot \left. \left(\displaystyle\sum_{i=1}^{3}\sum_{j=1}^{3}\left|\dfrac{\partial u_i}{\partial x_j}\right|\right)^2_{\text{iw}} \middle/ \left(\displaystyle\sum_{i=1}^{3}\sum_{j=1}^{3}\left|\dfrac{\partial u_i}{\partial x_j}\right|_{x_3=0}\right)_{\text{iw}} \right. \end{cases}, \tag{4}$$

where h_{iw} is the SSH amplitude of the mode-1 M_2 internal tide. $\left(\sum_{i=1}^{3} \sum_{j=1}^{3} \left| \dfrac{\partial u_i}{\partial x_j} \right| \right)_{iw}$ is the averaged velocity shear module of the

internal tides in a simple monochromatic form and can be calculated based on the unified linear theory under general ocean conditions (Yuan et al., 2011). The expression can be written as

135
$$\left(\sum_{i=1}^{3} \sum_{j=1}^{3} \left| \frac{\partial u_i}{\partial x_j} \right| \right)_{iw}^{2} = 2h_{iw} K_{iw}^2 \omega_{iw}^2 \frac{\left[\phi^2 \left(\omega_{iw} \right) - 1 \right]^2 \sin^2 \left[\int_{-H}^{x_3} \phi \left(\omega_{iw} \right) K_{iw} dx_3 \right] + 2\phi^2 \left(\omega_{iw} \right)}{\sin^2 \left[\int_{-H}^{0} \phi \left(\omega_{iw} \right) K_{iw} dx_3 \right]} ,$$
(5)

where

$$\phi \left(\omega_{iw} \right) = \sqrt{\frac{N^2 - \omega_{iw}^2}{\omega_{iw}^2 - f^2}} ,$$
(6)

where ω_{iw} is the M_2 tidal frequency, K_{iw} is the wave number. Under the influence of the Earth's rotation, the dispersion relation can be written as

140
$$\omega_{iw}^2 = K_{iw}^2 c_n^2 + f^2 ,$$
(7)

where f is the inertial frequency, c_n is the eigenvalue speed, which is the phase speed in a non-rotating fluid, the expression can be written as

$$c_n^2 = \left[\frac{\int_{-H}^{0} N \left(x_3 \right) dx_3}{n\pi} \right]^2 ,$$
(8)

where n is the mode number and set to be 1 here.

145 **2.4. Incorporating the Vertical Mixing Schemes into OGCMs**

The effects of the new vertical mixing schemes are introduced into the OGCMs. The modified equations can be written as

$$\begin{cases} \dfrac{\partial U_i}{\partial t} + U_j \dfrac{\partial U_i}{\partial x_j} = F + \Pi_U \\[2mm] \dfrac{\partial C}{\partial t} + U_j \dfrac{\partial C}{\partial x_j} = G + \Pi_C \end{cases} ,$$
(9)

where x_j (j = 1, 2, 3) are the x, y, and z axes of the Cartesian coordinates, U_i (i = 1, 2, 3) and C denote the mean velocity current

150 components and one of the two tracers including the potential temperature and salinity, respectively. The second terms on the left hand side of Eq. (9) are the advection ones. F represents the sum of the terms on the right hand side of the momentum equations including the Coriolis force, pressure gradient force, horizontal diffusion, molecular viscous force, and external forcing terms. G represents the sum of the terms on the right hand side of the tracer equations including horizontal diffusion,

molecular diffusivity force, and heat/fresh-water flux terms. Π_U and Π_C denote the modified vertical diffusive terms and can

155 be expressed as

$$
\begin{cases}
\Pi_U = \dfrac{\partial}{\partial x_3}\left(K_m \dfrac{\partial U_i}{\partial x_3}\right) + \dfrac{\partial}{\partial x_3}\left(B_{us} \dfrac{\partial U_i}{\partial x_3}\right) + \left(-B_{SM1} \dfrac{\partial U_i}{\partial x_1} - B_{SM2} \dfrac{\partial U_i}{\partial x_2}\right) + \dfrac{\partial}{\partial x_3}\left(B_{ui} \dfrac{\partial U_i}{\partial x_3}\right) \\
\Pi_C = \dfrac{\partial}{\partial x_3}\left(K_h \dfrac{\partial C}{\partial x_3}\right) + \dfrac{\partial}{\partial x_3}\left(B_{Ts} \dfrac{\partial C}{\partial x_3}\right) + \left(-B_{SM1} \dfrac{\partial C}{\partial x_1} - B_{SM2} \dfrac{\partial C}{\partial x_2}\right) + \dfrac{\partial}{\partial x_3}\left(B_{Ti} \dfrac{\partial C}{\partial x_3}\right)
\end{cases}
\tag{10}
$$

The new vertical diffusive terms Π_U and Π_C can be divided into four parts as shown in Eq. (10). The first term denotes the original diffusive term, where K_m and K_h are vertical eddy viscosity and diffusivity calculated by the classic Mellor-Yamada 2.5 (M-Y 2.5) scheme (Mellor and Yamada, 1982). The remaining terms represent the new diffusive terms generated by surface

160 waves and internal tides, which are described in Section 2.1 - 2.3.

3 Model Description and Numerical Experiment Design

3.1 Ocean circulation model

The three-demensional MASNUM ocean circulation model (Han and Yuan, 2014; Zhuang et al., 2018) is used to evaluate the effects of the NBSW- and IT-generated turbulent mixing and the WTFR-induced mixing. The two-level single-step

165 Eulerian forward-backward time-differencing scheme and the σ-Z-σ hybrid vertical coordinate are adopted in the MASNUM ocean model. The forward-backward scheme with a spatial smoothing method should be superior to the leapfrog scheme because of more stability and more computational efficiency (Han, 2014).

The model domain is in an area of 50° S - 30° N, 0° - 135° E (Fig. 1) with a horizontal resolution of 1°/6 by 1°/6. 5 surface σ layers, 31 intermediate Z layers and 3 bottom σ layers are used in the vertical direction in order to obtain the vertical

170 grid spacing with a high resolution in the upper ocean. The topography of the model is down sampled from the global General Bathymetric Chart of the Oceans 2008 (GEBCO_08) with a resolution of 1′ by 1′. The minimum depth is set to 5 m. The maximum depth is set to 5,000 m avoiding the artificial influences at deep water depths.

The initial temperature and salinity are interpolated based on the annually mean Levitus data with the horizontal resolution of 1° by 1° and 33 vertical layers. The initial velocities are set to 0. The lateral boundary conditions are obtained from the daily

175 global climatologic model results by the MASNUM model with the horizontal resolution of 1°/2 by 1°/2. The surface forcing including the momentum, heat and wind stress fluxes are calculated from the monthly mean surface fields of the National Centers for Environmental Prediction / National Center for Atmospheric Research (NCEP/NCAR) reanalysis data set from 1948 to 2021. The horizontal resolution is 1°/4 by 1°/4. The time step size of the barotropic mode is set to 30 s, while that of the baroclinic mode is 900 s. The model is integrated from the quiescent state for 10 climatological years. The simulated

180 temperature in the last 1 year are compared with the monthly World Ocean Atlas 2013 (WOA13) climatologic data, which can be regarded as the true solution of the climatological numerical experiments.

3.2 Wave spectrum model

The MASNUM wave spectrum model (Yang et al., 2019; Yuan et al., 1991, 1992) is used to simulate the parameters of the surface wave in the IO. The energy balanced equations are solved in the model based on the wave number spectrum space.

185   The characteristics inlaid scheme is adopted for the wave energy propagation to improve the original wave model (Yuan et al., 1992).

The model domain, the resolution, the topography and the surface wind stress flux data are consistent with that in the MASNUM ocean circulation model. The boundary conditions are from the JONSWAP spectrum (Hasselmann et al., 1973). The wave model is integrated from the quiescent state for 10 climatological years with the same period as the ocean circulation

190   model.

The wave spectrum $E(\vec{k})$ is calculated from the MASNUM wave model, and then ω_{sw}, K_{sw}, and h_{sw} can be estimated. Thus, the new mixing coefficients including B_{us}, B_{Ts}, B_{SM1}, B_{SM2}, B_{ui}, and B_{Ti} are calculated directly from Eqs. (1) - (4).

3.3 Experimental design

To assess the effects of the NBSW, WTFR and IT on the vertical mixing and the simulated thermal structure in the upper

195   ocean, five experiments (Table 1) are denoted as Exp 1 - 5 and designed as follows:

Exp 1 (benchmark experiment): The model is integrated with the classic M-Y 2.5 turbulence closure model (Mellor and Yamada, 1982), which is broadly used in the OGCMs.

Exp 2: Same as Exp 1, except with the classic M-Y 2.5 scheme and the NBSW-generated turbulent mixing scheme. This experiment is designed to evaluate the effect of the NBSW.

200   Exp 3: Same as Exp 1, except with the classic M-Y 2.5 scheme and the NBSW- and IT-generated turbulent mixing schemes. This experiment is designed to evaluate the effects of the NBSW and the IT. The experiment with the M-Y 2.5 scheme and the IT-generated turbulent mixing scheme (Exp 3.5) is omitted in this study, because the deviation of the temperature between Exp 1 and Exp 3.5 is too small. The possible reason is that the IT is often considered to enhance the vertical mixing in the ocean interior from the thermocline to the abyssal regions (Kunze et al., 2006; Munk and Wunsch, 1998;

205   Wunsch and Ferrari, 2004), therefore, it should be insufficient for the incorporation of only the IT into the M-Y 2.5 scheme to draw the warmer water from the surface into the interior. This implies that only the IT is unable to improve the upper-ocean simulation.

Exp 4: Same as Exp 1, except with the classic M-Y 2.5 scheme and the WTFR-induced mixing scheme. Comparisons between Exp 2 and Exp 4 are implemented to evaluate the two mechanisms that the surface waves affect the upper-ocean

210   vertical mixing.

Exp 5: Same as Exp 1, except with the classic M-Y 2.5 scheme and the NBSW- and IT-generated turbulent mixing and the WTFR-induced mixing schemes. This experiment is designed to evaluate the effects of the NBSW, the IT and the WTFR.

Table 1: Numerical experiment design

	NBSW	WTFR	IT
Exp 1	No	No	No
Exp 2	Yes	No	No
Exp 3	Yes	No	Yes
Exp 4	No	Yes	No
Exp 5	Yes	Yes	Yes

4. Results

215   In this section, the comparable results for the climatological temperature construction in the upper ocean are used to assess the effects of the NBSW, the IT, and the WTFR on the vertical mixing.

4.1 Comparison of vertical diffusive terms

As a typical example, the vertical distribution of the monthly mean vertical temperature diffusive terms in logarithmic scale along zonal transect of 10.5° S in January and July are shown in Figs. 2 and 3. As expressed in Eq. (10), the calculated

220   vertical diffusive term based on the M-Y 2.5 scheme, which is written as $\frac{\partial}{\partial x_3}\left(K_h \frac{\partial T}{\partial x_3}\right)$ (KHT for short) and calculated from

Exp 1, the NBSW-generated turbulent mixing scheme, which is written as $\frac{\partial}{\partial x_3}\left(B_{Ts} \frac{\partial T}{\partial x_3}\right)$ (BTST) and calculated from Exp 2,

the IT-generated turbulent mixing scheme, which is written as $\frac{\partial}{\partial x_3}\left(B_{Ti} \frac{\partial T}{\partial x_3}\right)$ (BTIT) and calculated from Exp 3 and the WTFR-

induced mixing scheme, which is written as $-B_{SM1}\frac{\partial T}{\partial x_1} - B_{SM2}\frac{\partial T}{\partial x_2}$ (BSMT) and calculated from Exp 4, are presented,

respectively. Figs. 2 and 3 show the comparisons among these diffusive terms along 10.5° S, which is a typical transect to

225   show the difference, in January and July. One can see that all of the terms decay with the depth below the sea surface. In January, BTST is > 10^{-2} °C s^{-1} in the upper-30 m layer of most regions, of which the values are too high to show in Figs. 2b and 3b, and obviously greater than other terms, implying that the NBSW-generated turbulent mixing is dominant in the layers with depths less than 30 m. Similar to BTST, BSMT (Fig. 2d) is also induced by NBSW and directly generated by the surface wave orbital velocity, but the values are about 4 to 6 orders smaller than those of BTST. However, in July, BSMT may affect

230   greater depths than BTST and KHT especially in some regions with large topographic relief. In the ocean interior with depths from 40 m to 130 m, BTIT (Fig. 2c) is about 10^{-6} °C s^{-1} and significantly higher than other three terms in some regions such

as the East Atlantic (5° E - 10° E), the West Indian Ocean (50° E - 70° E) and the West Pacific (122° E - 125° E) because of the effects of the IT.
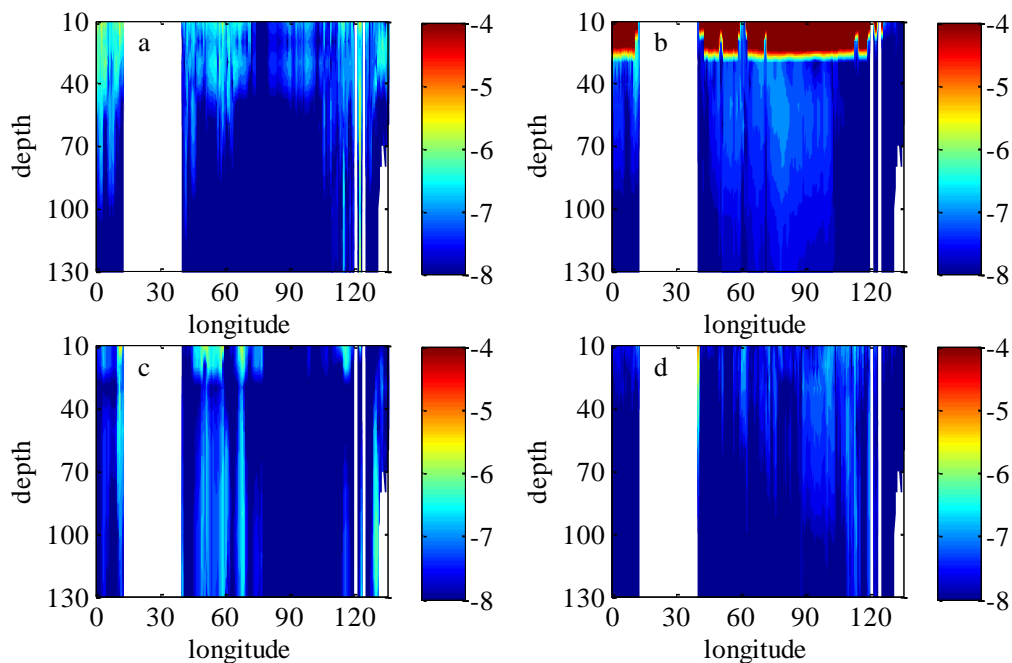
Figure 2: Vertical profiles of the monthly mean vertical temperature diffusive terms in logarithmic scale along 10.5° S in January, including the diffusive term based on the M-Y 2.5 scheme (a), the NBSW-generated turbulent mixing scheme (b), the IT-generated turbulent mixing scheme (c) and the WTFR-induced mixing scheme (d)
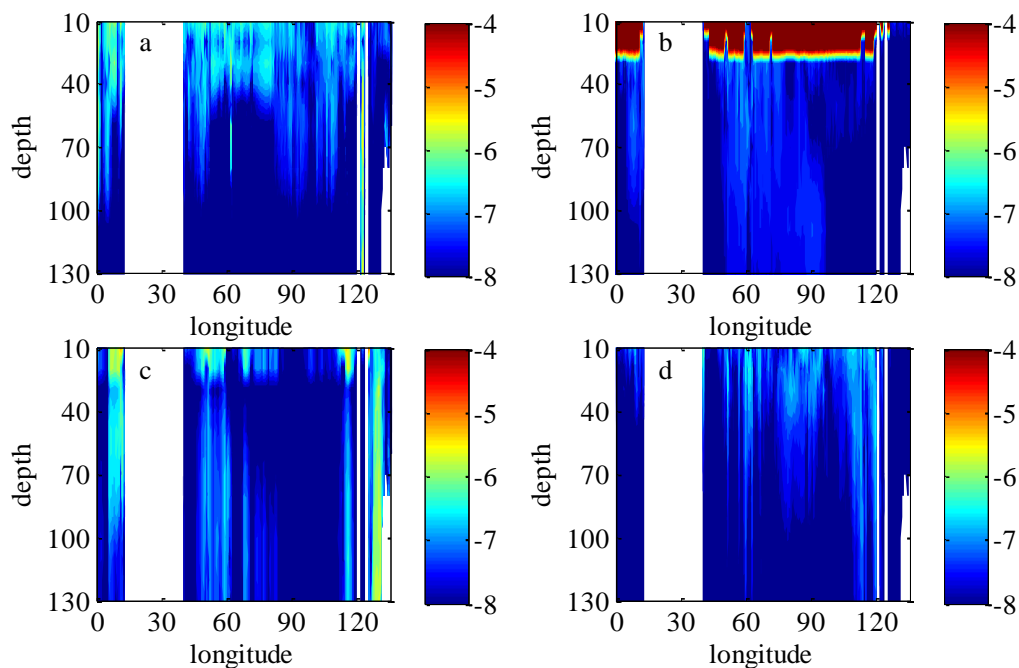
Figure 3: The same as Fig. 2, but in July

4.2 Effects on simulation of the vertical temperature structure

The climatologic experiments are designed in this study because of the NCEP monthly climatologic sea surface flux forcing fileds and the daily global climatologic lateral boundary conditions in the simulation, so the WOA13 monthly climatology data can be used in comparisons as a reference.

Figs. 4 - 7 show the comparisons of the upper-ocean temperature vertical structure between the WOA13 data and the model results of the five experiments along transects of 30.5° S and 7.5° N, corresponding to SIO and north of the Equatorial Indian Ocean (EIO), in January and July. One can see that the difference by subtracting the monthly mean results of Exp 1 from the monthly WOA13 data is the largest among the five experiments along the two transects in January and July. In the ocean interior, the temperature of Exp 1 is extremely lower than the WOA13 data, which implies that less surface water is transfered into the layers with depths from 30 m to 100 m in Exp 1 because of the insufficient vertical mixing process simulated by the classic M-Y 2.5 scheme. Compared with Exp 1, the difference for Exp 2 decreases remarkably, because the NBSW strengthens the vertical mixing and improve the upper-ocean simulation, which has been proved many times by previous studies (Huang et al., 2011; Lin et al., 2006; Qiao et al., 2016; Zhuang et al., 2020).
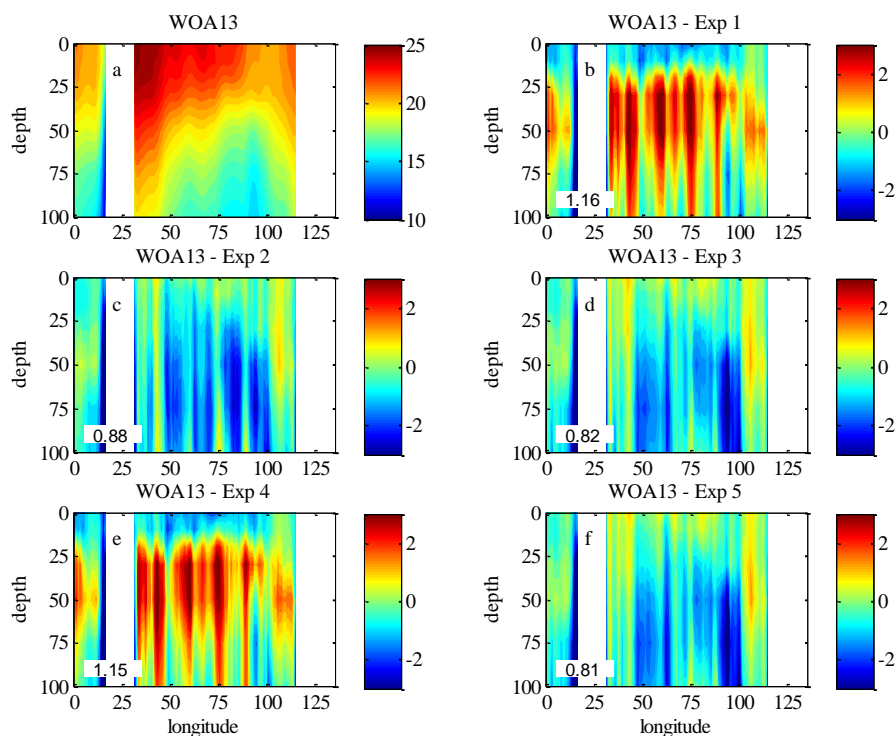
Figure 4: The vertical temperature profiles along 30.5° S in January. (a) The temperature structure from the monthly WOA13 data
255 **(units: °C). (b) - (f) The difference of the temperature calculated by subtracting the monthly mean results simulated in Exp 1 - Exp**
5 from the monthly WOA13 data, respectively. The RMSE of the temperature in the upper-100 m regions between the WOA13 data
and the model results are given. White areas correspond to the lands
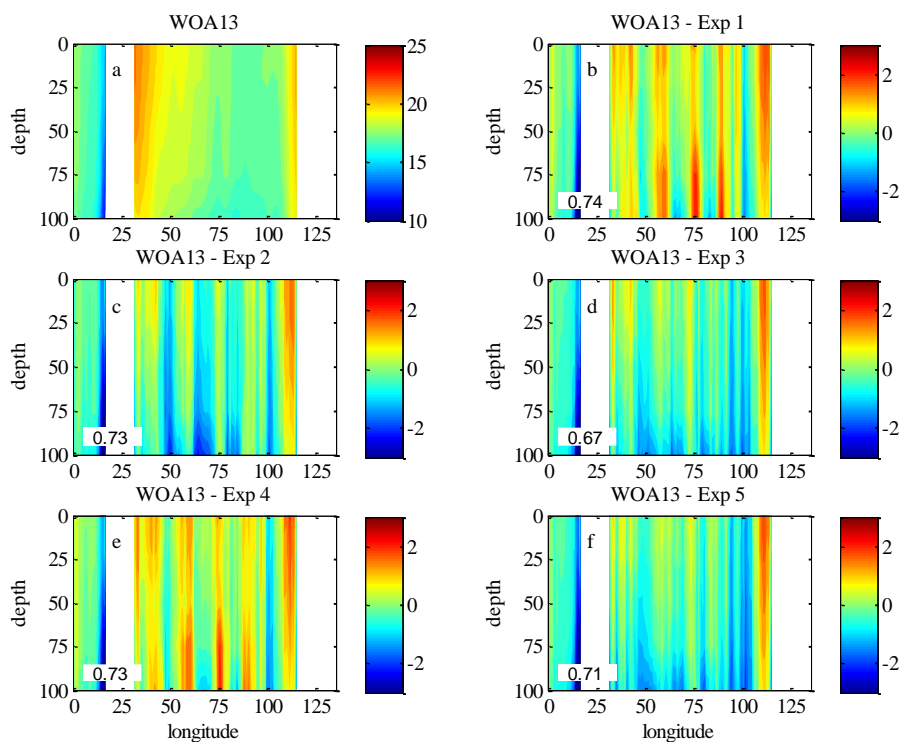
Figure 5: The same as Fig. 4, but in July
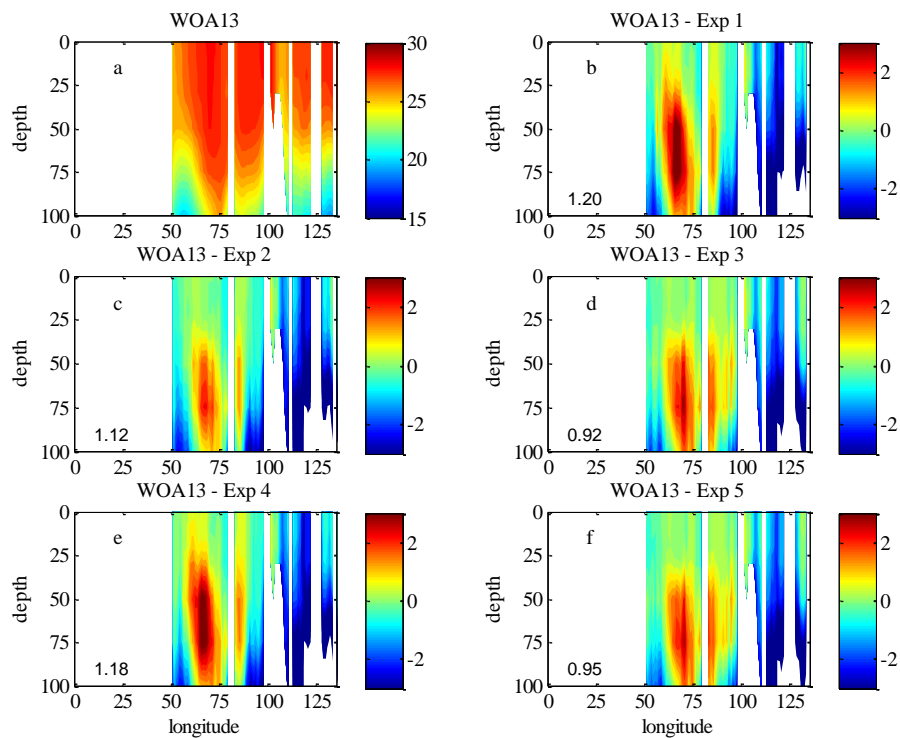
260

Figure 6: The same as Fig. 4, but along 7.5° N
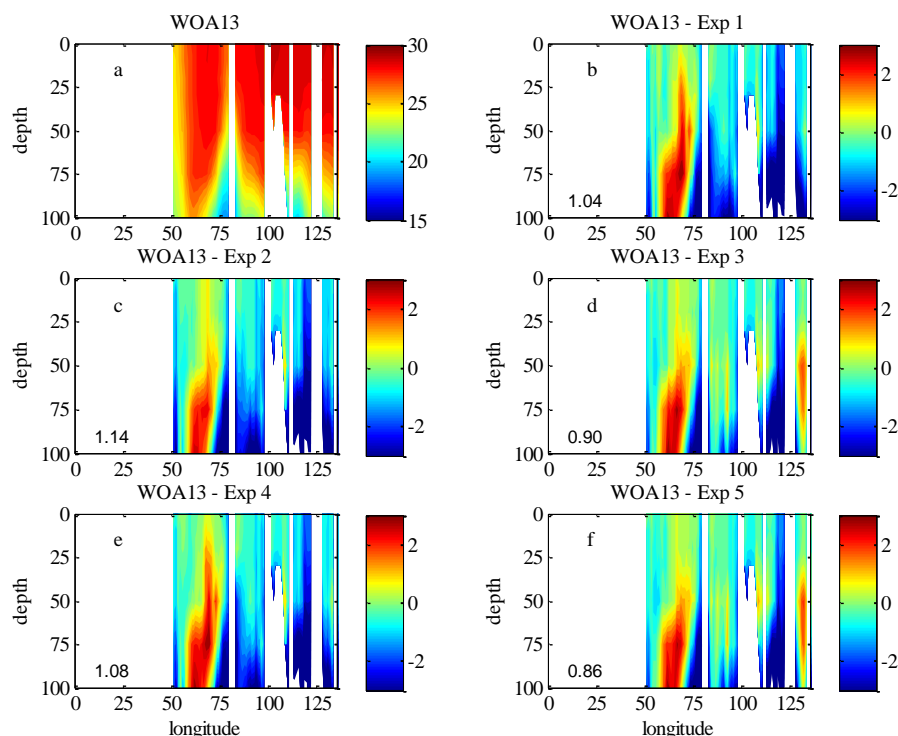
Figure 7: The same as Fig. 4, but along 7.5° N and in July

The difference for Exp 3 is much smaller than that of Exp 1 and Exp 2 because of the incorporation of the IT-generated

265 turbulent mixing, especially in the layers with depths between 20 m and 50 m. This implies that the IT strengthens the vertical

mixing of the ocean interior and improve the simulation further. It is worth noting that the experiment with the classic M-Y

2.5 scheme and the IT-generated turbulent mixing scheme is omitted, the reason is that the results have not been improved, if

only the IT-generated turbulent mixing is incorporated because the simulated surface mixing is insufficient, and even been

deteriorated in some regions because the colder water will be drawn from the lower layers with depths deeper than 100 m into

270 the upper ocean.

However, the simulation is slightly improved in Exp 4 compared with Exp 1 because the BSMT, which is induced by the

WTFR, is remarkably smaller than the BTW, so the WTFR-induced mixing is too insufficient to significantly improve

simulating the upper-ocean temperature structure. Similarly, there is less difference between Exp 3 and Exp 5, implying that

the effects of the WTFR on enhancing vertical mixing are much weaker than the NBSW in the surface layers and the IT in the

275 ocean interior.

Figure 8 shows the monthly variability of the root mean square errors (RMSEs) of the temperature in the upper-100 m

layers between the WOA13 data and the model results. The study area is divided into three zones (Zones 1 - 3 marked in Fig.

1), corresponding to the NIO, including the Arabian Sea and the Bay of Bengal, the Equatorial and tropical SIO and the SIO,

respectively.

280   In Zone 1, the RMSEs for Exp 2 are smaller than that for Exp 1 in all of the months, indicating the improvement of the NBSW on the upper-ocean simulation in the NIO. Compared with Exp 2, the RMSEs for Exp 3 are smaller in most of the months except November, December and January. This implies that the IT enhances the vertical mixing and improves the simulation further. The possible reason for little effects of the IT from November to January is that, on one hand, the mixed layer depths in the NIO are relatively shallower in boreal winter, so that the averaged velocity shear module of the internal

285   tides is smaller and the IT-induced mixing is weaker, on the other hand, the strength of the surface waves is more intensive, so the NBSW-induced mixing is relatively sufficient. The largest declines occurred in May, when the RMSE decreasd 14.0% from 1.72 °C (Exp 1) to 1.49 °C (Exp 2), and 19.1% from 1.72 °C (Exp 1) to 1.40 °C (Exp 3).

        In Zone 2, the NBSW is ineffective, because the RMSEs for Exp 2 are almost equal to, even larger than, those for Exp 1. This is a long-standing issue about the trivial effects of the NBSW in the tropical area (Qiao et al., 2010; Zhuang et al., 2020),

290   implying that only the NBSW should be not enough to improve the tropical simulation. To solve this issue, the coupled atmosphere-wave-ocean-ice modeling is one of the solution (Song et al., 2012; Wang et al., 2019). Another way is incorporation of the additional mechanism into the OGCMs, such as the IT-generated turbulent mixing added in Exp 3 and Exp 5. The RMSEs for Exp 3 are obviously smaller than that for Exp 1 and Exp 2 in the whole climatologic year except March, implying that the combination of the NBSW and the IT is able to improve the simulation of the temperature structure in the

295   tropical area. Additionally, the RMSEs in Zone 2 are smaller than that in Zones 1 and 3 on the whole, the RMSEs in Zone 2 for Exp 3 and Exp 5 are even less than 0.9 °C in half of the climatologic year, indicating much accurate simulation in the tropical area.

        In Zone 3, the results are similar to that in Zone 1, the RMSEs for Exp 2 are smaller than that for Exp 1 in most months, and the RMSEs for Exp 3 are the smallest ones among the first three experiments. The largest declines occurred in January,

300   when the RMSE decreases 20.8% from 1.50 °C (Exp 1) to 1.18 °C (Exp 2), and 25.7% from 1.50 °C (Exp 1) to 1.11 °C (Exp 3). The situation also indicates the significant improvements of the combination of the NBSW and the IT in simulating the upper-ocean temperature structure.

        Furthermore, in Zones 1 - 3, the effects of WTFR are much weaker and similar to that in Figs. 4 - 7, because the RMSEs for Exp 4/5 are almost equal to, and even larger than, that for Exp 1/3. The possible reason is that the values of the WTFR-

305   induced diffusion terms are about 4 to 6 orders smaller than NBSW, which are too low to enhance the vertical mixing especially in the surface layers.
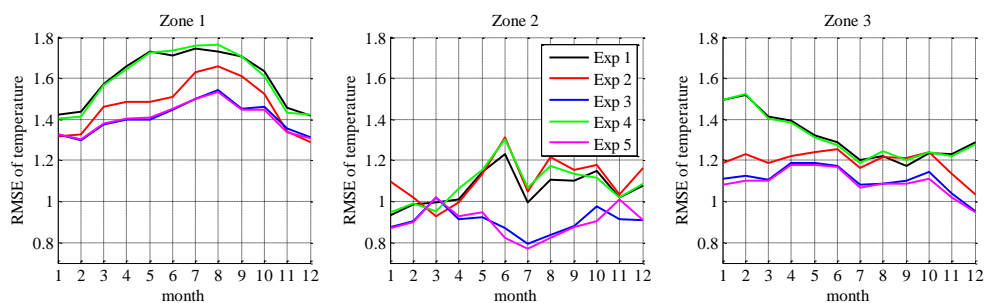
Figure 8: Variation of the RMSE of the temperature between the simulated monthly mean results in the five experiments and the monthly WOA13 data in Zones 1 - 3 (shown in Fig. 1)

310 **4.3 Effects on simulation of the mixed layer depth**

The mixed layer (ML), which is characterized by a quasi-uniform temperature and salinity, is crucial in understanding the physical processes in the upper ocean. The MLD variability is influenced by many processes including wind-induced turbulence, surface warming or cooling, air-sea heat exchange and turbulence-wave interaction (Abdulla et al., 2019; Chen et al., 1994; de Boyer Montégut et al., 2004; Kara et al., 2003). There are different methods to define the MLD (Kara et al., 2003).

315 In this study, the MLD is defined as a depth where the temperature is lower than the SST by 1.0 °C and used to show the upper-ocean thermal structure.

Figure 9 shows the comparisons of the MLDs between the WOA13 data and the model results in January. The MLDs for Exp 1 are generally shallower than the WOA13 in the whole IO and the Southern Ocean because of insufficient simulated mixing processes. Comparisons among the MLDs for Exp 1 – Exp 3 show that the NBSW and IT may enhance the upper-

320 ocean mixing and make the simulated MLDs closer to the WOA13 data. The MLs for Exp 2 and Exp 3 are extremely deepened especially in the tropical IO and the Southern Ocean. The RMSEs of the MLDs between the WOA13 data and the model results decrease 13.2% and 14.6% from 21.9 m (Exp 1) to 19.0 m (Exp 2) and to 18.7 m (Exp 3), respectively. However, the effects of the WTFR seem to be trivial in the whole area, because there is almost no improvement from Exp 4/5 to Exp 1/3. The RMSEs for Exp 4/5 are larger than that for Exp 1/3, and the larger deviations in Exp 4/5 mostly occur in the Southern Ocean,

325 implying that the WTFR does not work well in the Southern Ocean in austral winter.
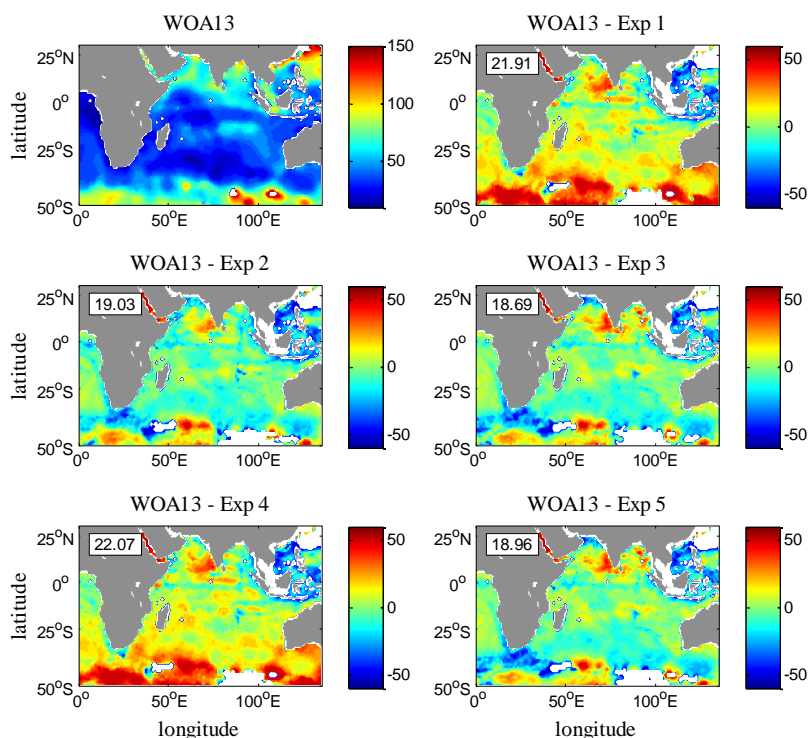
Figure 9: The distribution of the MLD calculated from WOA13 data and the differences of the MLD between the WOA13 data and the results simulated in Exp 1 – Exp 5. RMSEs of the MLD are shown on the upper left corner of the sub-figures. Dark and white areas correspond to the lands and the calculated MLDs are deeper than 150 m, respectively

5. Discussion

We evaluate the impacts of three different mixing schemes, including the NBSW-generated turbulent mixing, the WTFR-induced mixing, and the IT-generated turbulent mixing, on the upper-ocean thermal structure simulation in the IO. The comparisons of the temperature structure and the MLDs between the WOA13 data, which is regarded as the observations, and the model results imply that the simulation is significantly improved by incorporating the NBSW- and IT-generated turbulent mixing into the MASNUM ocean circulation model, but the effects of the WTFR is trivial, the simulated MLDs are even deteriorated in some regions. However, based on numerical experiments, Yang et al. (2019) demonstrated that the WTFR may play an important role in the SST cooling, if the wind and surface waves are strong. During the period of the tropical cyclone Nepartak passage, the simulated SST cooling distribution and the cooling amplitude are more consistent with the observations, if the WTFR-induced mixing scheme is incorporated, which present waring/cooling effects on the left/right sides of the typhoon track (Yu et al., 2020). The effects of the WTFR under the typhoon conditions will be further examined in the future work.

In addition, the three mixing schemes are incorporated into the MASNUM model as a part of the vertical diffusive terms, thus avoiding the issues that may be resulted from adding the mixing coefficients to those from the M-Y 2.5 scheme directly. The analysis of the numerical results indicates that the NBSW (and WTFR, sometimes) leads to improve simulations of upper-ocean temperature structure and MLDs due to the enhanced mixing that draws the warmer water from the surface to the subsurface layers with depths from about 10 m to 40 m, then the IT, which can improve the simulations further, may enhance the mixing that draws the warmer water from the subsurface layers to the ocean interior (Fig. 10). In summary, the combination of the NBSW- and IT-generated turbulent mixing results in a better match with the observations of upper-ocean temperature structure and MLDs.
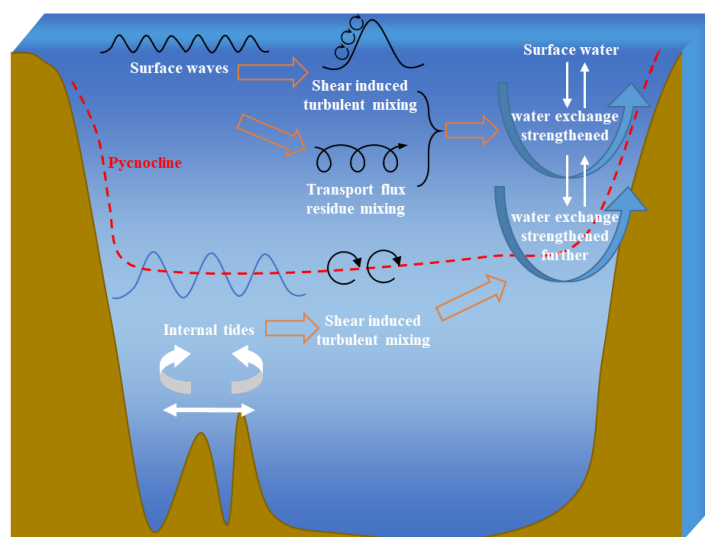
Figure 10: Sketch of the enhancing processes of the vertical mixing induced by three different mechanisms, including the NBSW-generated turbulent mixing, the WTFR-induced mixing, and the IT-generated turbulent mixing

It is worth noting that the circulation and the temperature structure of the IO have been not yet characterized by the ocean model in the present study because of the non-ignorable difference between the WOA13 data and the simulation results. The RMSEs in the NIO, including the Arabian Sea and the Bay of Bengal, are even generally larger than 1.2 ℃. Therefore, higher horizontal resolution and more vertical layers, on one hand, will be designed in following experiments to describe the finer structure and features of the IO, on the other hand, the surface forcing and the lateral boundary conditions with higher spatio- and temporal-resolution, such as the ERA5 hourly reanalysis data (https://cds.climate.copernicus.eu/cdsapp#!/dataset/reanalysis-era5-single-levels?tab=form), the Climate Forecast System Version 2 (CFSv2) (http://rda.ucar.edu/datasets/ds094.0/) and the global HYbrid Coordinate Ocean Model/Navy Coupled Ocean Data Assimilation (HYCOM/NCODA) product (https://www.hycom.org/data/glba0pt08/expt-90pt8), will be used to simulate the IO more accurately.

6. Conclusions

This study uses the MASNUM ocean circulation model for testing and validating the effects of three different mixing
365   schemes, including the NBSW-generated turbulent mixing, the WTFR-induced mixing and the IT-generated turbulent mixing,
on the upper-ocean thermal structure simulation in the IO. The major findings aresummarized as follows.

1). The diffusive terms calculated by the NBSW-generated turbulent mixing is dominant if the depth is less than 30 m,
while the WTFR-induced mixing is extremely weak because the values are about 4 to 6 orders smaller than the NBSW. In the
ocean interior with depths from 40 m to 130 m, the diffusive terms calculated by the IT-generated turbulent mixing are the
370   largest ones in regions with large topographic relief.

2). The effects of these schemes on the upper-ocean simulation are tested. The results show that the simulated thermal
structure and MLDs are both improved by the NBSW, because of the enhanced mixing in the sea surface, while the effects of
the WTFR is trivial.

3). The IT may strengthen the vertical mixing of the ocean interior and improve the simulation further. In summary, the
375   combination of the NBSW and IT may strengthen the vertical mixing and improve the upper-ocean simulation.

Appendix A: The velocity shear module of the internal tide

The internal-tide-induced mixing plays an important role in the vertical and horizontal distribution of water mass
properties. Based on the Navier-Stokes equations, the solvability simplification is realized based on the spatio-temporal scale,
controlling mechanism and actual characteristics of the internal tides. The internl tide is considered to be weakly nolinear, the
380   shear terms of the larger-scale motions in the equations are linear approximately, and the molecular and turbulent mixing terms
in the equations are too small to be ignored. The f-plane and layered approximation for the larger-scale motions are also
adopted into the equations. Thus, the simplified equations can be written as

$$\frac{\partial u_{IT1}}{\partial x_1} + \frac{\partial u_{IT2}}{\partial x_2} + \frac{\partial u_{IT3}}{\partial x_3} + \gamma u_{IT1} = 0 \ , \tag{11}$$

$$\frac{\partial u_{IT1}}{\partial t} - f u_{IT2} - 2U_1\gamma u_{IT2} = -\frac{\partial}{\partial x_1}\left(\frac{p_{IT}}{\rho_0}\right), \tag{12}$$

385   $$\frac{\partial u_{IT2}}{\partial t} + \left(f + 2\gamma U_2 + \frac{\partial U_2}{\partial x_1}\right)u_{IT1} + \frac{\partial U_2}{\partial x_3}u_{IT3} = -\frac{\partial}{\partial x_2}\left(\frac{p_{IT}}{\rho_0}\right), \tag{13}$$

$$\frac{\partial u_{IT3}}{\partial t} = -\frac{\partial}{\partial x_3}\left(\frac{p_{IT}}{\rho_0}\right) - g\left(\frac{\rho_{IT}}{\rho_0}\right), \tag{14}$$

$$\frac{\partial}{\partial t}\left(\frac{\rho_{IT}}{\rho_0}\right) + \frac{\partial}{\partial x_1}\left(\frac{\rho_{IT}}{\rho_0}\right)u_{IT1} + \frac{\partial}{\partial x_3}\left(\frac{\rho_{IT}}{\rho_0}\right)u_{IT3} = 0 \ , \tag{15}$$

where u_{ITi} (i=1, 2, 3), ρ_{IT} and p_{IT} denote the three dimensional velocity, density and pressure of the internal tide, respectively.
f is the Coriolis parameter, γ is regarded as the curvature of the larger-scale motions including mesoscale eddies, gyre and so

390   on. U_i represent the velocity of the larger-scale motions. The Fourier kernel function is used to transform the differential

equations (11) to (15) to the algebraic equations, for example, the relation between u_{IT1} and its Fourier kernel function μ_{IT1}

can be expressed as

$$u_{IT1} = \iint_k \eta_{IT} \mu_{IT1} \exp\left\{i\left(k_1 x_1 + k_2 x_2 - \omega t\right)\right\} dk_1 dk_2 , \qquad (16)$$

where η_{IT} is the SSH amplitude of the internal tide, ω is the frequency. The dispersion relation between the frequency and the

395   wavenumber can be written as

$$\omega^2 \left(\frac{N_0^2}{\omega^2} - 1\right)^{1/2} = g\left(\frac{\rho_{IT}}{\rho_0}\right) k \frac{\sin\left\{\int_{-H}^{0}\left(\frac{N^2}{\omega^2} - 1\right)^{1/2} k dx_3\right\}}{\cos\left\{\int_{-H}^{0}\left(\frac{N^2}{\omega^2} - 1\right)^{1/2} k dx_3\right\}} , \qquad (17)$$

$$\frac{\partial \omega}{\partial x_3} = 0 . \qquad (18)$$

Based on the analytical expression of the three dimensional velocity (derived from the Fourier kernel functions) and Eqs. (17)

and (18), the velocity shear module can be expressed analytically as

400
$$\left(\sum_{i=1}^{3}\sum_{j=1}^{3}\left|\frac{\partial u_{ITi}}{\partial x_j}\right|\right)^2 = \left\{2\iint_k \eta_{IW} k^2 \omega^2 \frac{\left(\frac{N^2}{2\omega^2}\right)^2 - \left(\frac{N^2}{2\omega^2} - 1\right)^2 \cos\left\{2\int_{-H}^{x_3}\left(\frac{N^2}{\omega^2} - 1\right)^{1/2} k dx_3\right\}}{\sin^2\left\{\int_{-H}^{0}\left(\frac{N^2}{\omega^2} - 1\right)^{1/2} k dx_3\right\}} dk_1 dk_2\right\}^{1/2} , \qquad (19)$$

which is consistent with Eq. (5). Similar to Gregg (1989) and Gregg and Kunze (1991), the mixing terms including the viscosity

and diffusivity can be calculated from the velocity shear modules as shown in Eq. (4).

Code and data availability. The MASNUM ocean circulation and wave spectrum models can be downloaded at

405   https://github.com/jumpen/MASNUM-ocean-circulation-model and https://github.com/jumpen/MASNUM-wave-model,

respectively. The global GEBCO_08 data can be downloaded from

https://www.gebco.net/data_and_products/gridded_bathymetry_data/#global. The WOA13 climatologic data can be

downloaded from https://www.nodc.noaa.gov/OC5/woa13/. The annually mean Levitus data can be downloaded from

http://iridl.ldeo.columbia.edu/SOURCES/.LEVITUS94/.ANNUAL/. The NCEP/NCAR reanalysis data can be downloaded

410   from https://psl.noaa.gov/data/gridded/data.ncep.reanalysis.surfaceflux.html. The simulation data in this studycan be

downloaded at: https://github.com/jumpen/Simulation-data-for-the-Indian-Ocean.

Author contributions. ZZ wrote the paper with the help of all the coauthors. QZ, YY and ZS provided constructive feedback

on the manuscript. YY designed and developed the theoretical basis of the improved vertical mixing scheme. CZ, XZ, TZ and

415   JX gave help and advice in data processing and numerical experiments.

Competing interests. The authors declare that they have no conflict of interest.

Financial support. This work is supported by the National Natural Science Foundation of China (Grant No. 42106031), Basic
420 Scientific Fund for National Public Research Institutes of China (Grant No. 2020Q04), National Programme on Global Change
and Air-sea Interactions (phase II) - "Distribution and Evolution of Ocean Dynamic Processes" (Grant No. GASI-04-WLHY-
01), National Program on Global Change and Air-Sea Interaction (Phase II) - "Parameterization assessment for interactions of
the ocean dynamic system" (Grant No. GASI-04-WLHY-02), Shandong Provincial Natural Science Foundation, China (Grant
No. ZR202102240074), National Natural Science Foundation of China (Grant No. 42006008).
425

References

Abdulla, C. P., Alsaafani, M. A., Alraddadi, T. M., and Albarakati, A. M.: Climatology of mixed layer depth in the Gulf of
Aden derived from in situ temperature profiles, Journal of Oceanography, 75, 335-347, 10.1007/s10872-019-00506-9, 2019.
430 Agrawal, Y. C., Terray, E. A., Donelan, M. A., Hwang, P. A., Williams, A. J. I., Drennan, W. M., and Krtaigorodskii, S. A.:
Enhanced dissipation of kinetic energy beneath surface waves, Nature, 359, 219-220, 1992.
Aijaz, S., Ghantous, M., Babanin, A. V., Ginis, I., Thomas, B., and Wake, G.: Nonbreaking wave-induced mixing in upper
ocean during tropical cyclones using coupled hurricane-ocean-wave modeling, Journal of Geophysical Research Oceans, 122,
3939-3963, 2017.
435 Alford, M. H.: Internal Swell Generation: The Spatial Distribution of Energy Flux from the Wind to Mixed Layer Near-Inertial
Motions,   Journal   of   Physical   Oceanography,   31,   2359-2368,   https://doi.org/10.1175/1520-
0485(2001)031<2359:Isgtsd>2.0.Co;2, 2001.
Anoop, T. R., Kumar, V. S., Shanas, P. R., and Johnson, G.: Surface Wave Climatology and Its Variability in the North Indian
Ocean Based on ERA-Interim Reanalysis, Journal of Atmospheric and Oceanic Technology, 32, 1372-1385,
440 https://doi.org/10.1175/jtech-d-14-00212.1, 2015.
Ansong, J. K., Arbic, B. K., Alford, M. H., Buijsman, M. C., Shriver, J. F., Zhao, Z., Richman, J. G., Simmons, H. L., Timko,
P. G., Wallcraft, A. J., and Zamudio, L.: Semidiurnal internal tide energy fluxes and their variability in a Global Ocean Model
and moored observations, Journal of Geophysical Research: Oceans, 122, 1882-1900, https://doi.org/10.1002/2016jc012184,
2017.
445 Babanin, A. V.: Similarity Theory for Turbulence, Induced by Orbital Motion of Surface Water Waves, 24th International
Congress of Theoretical and Applied Mechanics, Elsevier B. V., 20, 99-102, https://doi.org/10.1016/j.piutam.2017.03.014,
2017.

Babanin, A. V., and Haus, B. K.: On the Existence of Water Turbulence Induced by Nonbreaking Surface Waves, Journal of Physical Oceanography, 39, 2675-2679, 2009.

450 Baumert, H., Simpson, J., and Sundermann, J.: Marine turbulence: theories, observations and models, Cambridge University Press, Cambridge, 314 pp., 2005.

Chen, D., Busalacchi, A. J., and Rothstein, L. M.: The roles of vertical mixing, solar radiation, and wind stress in a model simulation of the sea surface temperature seasonal cycle in the tropical Pacific Ocean, Journal of Geophysical Research, 99, 20345-20359, https://doi.org/10.1029/94jc01621, 1994.

455 Dai, D., Qiao, F., Sulisz, W., Lei, H., and Babanin, A.: An Experiment on the Nonbreaking Surface-Wave-Induced Vertical Mixing, Journal of Physical Oceanography, 40, 2180-2188, 2010.

de Boyer Montégut, C., Madec, G., Fischer, A. S., Lazar, A., and Iudicone, D.: Mixed layer depth over the global ocean: An examination of profile data and a profile-based climatology, Journal of Geophysical Research, 109, C12003, https://doi.org/10.1029/2004jc002378, 2004.

460 Donelan, M. A.: Air-water exchange processes, in: Physical Processes in Lakes and Oceans, Coastal and Estuarine Study, edited by: Imberger, J., American Geophysical Union, Washington, D. C., 19-36, 1998.

Ezer, T.: On the seasonal mixed layer simulated by a basin-scale ocean model and the Mellor-Yamada turbulence scheme, Journal of Geophysical Research Oceans, 105, 16843-16855, 2000.

Furuichi, N., Hibiya, T., and Niwa, Y.: Model-predicted distribution of wind-induced internal wave energy in the world's 465 oceans, Journal of Geophysical Research, 113, C09034, https://doi.org/10.1029/2008jc004768, 2008.

Gregg, M. C.: Scaling turbulent dissipation in the thermocline, Journal of Geophysical Research: Oceans, 94, 9686-9698, https://doi.org/10.1029/JC094iC07p09686, 1989.

Gregg, M. C., and Kunze, E.: Shear and strain in Santa Monica Basin, Journal of Geophysical Research, 96, 16709-16719, https://doi.org/10.1029/91jc01385, 1991.

470 Gregg, M. C., Sanford, T. B., and Winkel, D. P.: Reduced mixing from the breaking of internal waves in equatorial waters, Nature, 422, 513-515, https://doi.org/10.1038/nature01507, 2003.

Han, L.: A two-time-level split-explicit ocean circulation model (MASNUM) and its validation, Acta Oceanologica Sinica, 33, 11-35, 2014.

Han, L., and Yuan, Y. L.: An ocean circulation model based on Eulerian forward-backward difference scheme and three-
475 dimensional, primitive equations and its application in regional simulations, Journal of Hydrodynamics, 26, 37-49, 2014.

Hasselmann, K., Barnett, T. P., Bouws, E., Carlson, H., Cartwright, D. E., Enke, K., Ewing, J. A., Gienapp, H., Hasselmann, D. E., Kruseman, P., Meerburg, A., Muller, P., Olbers, D. J., Richter, K., Sell, W., and Walden, H.: Mensurements of wind-wave growth and swell decay during the joint north sea wave project (JONSWAP), Deutche Hydrological Institute, Hamburg, 93 pp., 1973.

480 Huang, C., and Qiao, F.: Wave-turbulence interaction and its induced mixing in the upper ocean, Journal of Geophysical Research, 115, 1-12, https://doi.org/10.1029/2009jc005853, 2010.

Huang, C., Qiao, F., Song, Z., and Ezer, T.: Improving simulations of the upper ocean by inclusion of surface waves in the Mellor-Yamada turbulence scheme, Journal of Geophysical Research Oceans, 116, C01007, 2011.

Huussen, T. N., Naveira-Garabato, A. C., Bryden, H. L., and McDonagh, E. L.: Is the deep Indian Ocean MOC sustained by

485   breaking internal waves?, Journal of Geophysical Research: Oceans, 117, C08024, https://doi.org/10.1029/2012jc008236, 2012.

Kantha, L., Tamura, H., and Miyazawa, Y.: Comment on "wave-turbulence interaction and its induced mixing in the upper ocean" by Huang and Qiao, Journal of Geophysical Research Oceans, 119, 1510-1515, 2014.

Kara, A. B., Wallcraft, A. J., and Hurlburt, H. E.: Climatological SST and MLD predictions from a global layered ocean model

490   with an embedded mixed layer, Journal of Atmospheric and Oceanic Technology, 20, 1616-1632, 2003.

Kumar, E. D., Sannasiraj, S. A., Sundar, V., and Polnikov, V. G.: Wind-Wave Characteristics and Climate Variability in the Indian Ocean Region Using Altimeter Data, Marine Geodesy, 36, 303-318, https://doi.org/10.1080/01490419.2013.771718, 2013.

Kumar, V. S., Joseph, J., Amrutha, M. M., Jena, B. K., Sivakholundu, K. M., and Dubhashi, K. K.: Seasonal and interannual

495   changes of significant wave height in shelf seas around India during 1998–2012 based on wave hindcast, Ocean Engineering, 151, 127-140, https://doi.org/10.1016/j.oceaneng.2018.01.022, 2018.

Kunze, E.: Internal-Wave-Driven Mixing: Global Geography and Budgets, Journal of Physical Oceanography, 47, 1325-1345, 10.1175/jpo-d-16-0141.1, 2017.

Kunze, E., Firing, E., Hummon, J. M., Chereskin, T. K., and Thurnherr, A. M.: Global Abyssal Mixing Inferred from Lowered

500   ADCP Shear and CTD Strain Profiles, Journal of Physical Oceanography, 36, 1553-1576, https://doi.org/10.1175/jpo2926.1, 2006.

Li, M., and Garrett, C.: Mixed Layer Deepening Due to Langmuir Circulation, Journal of Physical Oceanography, 27, 121-132, https://doi.org/10.1175/1520-0485(1997)027<0121:Mlddtl>2.0.Co;2, 1997.

Li, Q., and Fox-Kemper, B.: Assessing the Effects of Langmuir Turbulence on the Entrainment Buoyancy Flux in the Ocean

505   Surface Boundary Layer, Journal of Physical Oceanography, 47, 2863-2886, https://doi.org/10.1175/jpo-d-17-0085.1, 2017.

Lin, X., Xie, S. P., Chen, X., and Xu, L.: A well-mixed warm water column in the central Bohai Sea in summer: effects of tidal and surface wave mixing, Journal of Geophysical Research Oceans, 111, C11017, 2006.

Mellor, G. L., and Yamada, T.: Development of a turbulence closuremodel for geophysical fluid problems, Reviews of geophysics and space physics, 20, 851-875, 1982.

510   Munk, W. H., and Wunsch, C.: Abyssal recipes II: energetics of tidal and wind mixing, Deep Sea Research Part I: Oceanographic Research Papers, 45, 1977-2010, https://doi.org/10.1016/s0967-0637(98)00070-3, 1998.

Polzin, K. L., Naveira Garabato, A. C., Huussen, T. N., Sloyan, B. M., and Waterman, S.: Finescale parameterizations of turbulent dissipation, Journal of Geophysical Research: Oceans, 119, 1383-1419, https://doi.org/10.1002/2013jc008979, 2014.

Qiao, F., Yuan, Y., Deng, J., Dai, D., and Song, Z.: Wave–turbulence interaction-induced vertical mixing and its effects in

515   ocean and climate models, Philosophical Transactions A, 374, 1-20, http://doi.org/10.1098/rsta.2015.0201, 2016.

Qiao, F., Yuan, Y., Ezer, T., Xia, C., Yang, Y., Lü, X., and Song, Z.: A three-dimensional surface wave–ocean circulation coupled model and its initial testing, Ocean Dynamics, 60, 1339-1355, https://doi.org/10.1007/s10236-010-0326-y, 2010.

Qiao, F., Yuan, Y., Yang, Y., Zheng, Q., and Jian, M.: Wave-induced mixing in the upper ocean: Distribution and application to a global ocean circulation model, Geophysical Research Letters, 31, 293-317, 2004.

520 Ray, R. D., and Mitchum, G. T.: Surface manifestation of internal tides generated near Hawaii, Geophysical Research Letters, 23, 2101-2104, https://doi.org/10.1029/96gl02050, 1996.

Scott, R. B., Goff, J. A., Naveira Garabato, A. C., and Nurser, A. J. G.: Global rate and spectral characteristics of internal gravity wave generation by geostrophic flow over topography, Journal of Geophysical Research, 116, https://doi.org/10.1029/2011jc007005, 2011.

525 Shay, T. J., and Gregg, M. C.: Convectively Driven Turbulent Mixing in the Upper Ocean, Journal of Physical Oceanography, 16, 1777-1798, https://doi.org/10.1175/1520-0485(1986)016<1777:Cdtmit>2.0.Co;2, 1986.

Shi, Y., Wu, K., and Yang, Y.: Preliminary Results of Assessing the Mixing of Wave Transport Flux Residualin the Upper Ocean with ROMS, Journal of Ocean University of China, 15, 193-200, 2016.

Shriver, J. F., Arbic, B. K., Richman, J. G., Ray, R. D., Metzger, E. J., Wallcraft, A. J., and Timko, P. G.: An evaluation of the
530 barotropic and internal tides in a high-resolution global ocean circulation model, Journal of Geophysical Research: Oceans, 117, C10024, https://doi.org/10.1029/2012jc008170, 2012.

Song, Z., Liu, H., and Chen, X.: Eastern equatorial Pacific SST seasonal cycle in global climate models: from CMIP5 to CMIP6, Acta Oceanologica Sinica, 39, 50-60, https://doi.org/10.1007/s13131-020-1623-z, 2020.

Song, Z., Qiao, F., and Song, Y.: Response of the equatorial basin-wide SST to non-breaking surface wave-induced mixing in
535 a climate model: An amendment to tropical bias, Journal of Geophysical Research Oceans, 117, C00J26, 2012.

Song, Z., Qiao, F., Yang, Y., and Yuan, Y.: An improvement of the too cold tongue in the tropical Pacific with the development of an ocean-wave-atmosphere coupled numerical model, Progress in Natural ence:Materials International, 17, 576-583, 2007.

Umlauf, L., and Burchard, H.: Marine Turbulence, 3rd ed, Online Available:https://www.io-warnemuende.de/tl_files/staff/umlauf/turbulence/turbulence.pdf, 79 pp., 2020.

540 Vic, C., Naveira Garabato, A. C., Green, J. A. M., Waterhouse, A. F., Zhao, Z., Melet, A., de Lavergne, C., Buijsman, M. C., and Stephenson, G. R.: Deep-ocean mixing driven by small-scale internal tides, Nat Commun, 10, 2099, https://doi.org/10.1038/s41467-019-10149-5, 2019.

Wang, S., Wang, Q., Shu, Q., Scholz, P., Lohmann, G., and Qiao, F.: Improving the Upper-ocean Temperature in an Ocean Climate Model (FESOM 1.4): Shortwave Penetration vs. Mixing Induced by Non-breaking Surface Waves, Journal of
545 Advances in Modeling Earth Systems, 11, 1-13, 2019.

Wang, W., and Huang, R. X.: Wind energy input to the surface waves, Journal of Physical Oceanography, 34, 1276-1280, 2004.

Whalen, C. B., de Lavergne, C., Naveira Garabato, A. C., Klymak, J. M., MacKinnon, J. A., and Sheen, K. L.: Internal wave-driven mixing: governing processes and consequences for climate, Nature Reviews Earth & Environment, 1, 606-621,
550   https://doi.org/10.1038/s43017-020-0097-z, 2020.

Wright, C. J., Scott, R. B., Ailliot, P., and Furnival, D.: Lee wave generation rates in the deep ocean, Geophysical Research Letters, 41, 2434-2440, 10.1002/2013gl059087, 2014.

Wunsch, C.: Baroclinic Motions and Energetics as Measured by Altimeters, Journal of Atmospheric and Oceanic Technology, 30, 140-150, https://doi.org/10.1175/jtech-d-12-00035.1, 2013.

555   Wunsch, C., and Ferrari, R.: Vertical mixing, energy, and the general circulation of the oceans, Annual review of fluid mechanics, 36, 281-314, 2004.

Xia, C., Qiao, F., Yang, Y., Ma, J., and Yuan, Y.: Three-dimensional structure of the summertime circulation in the Yellow Sea from a wave-tidecirculation coupled model, Journal of Geophysical Research Oceans, 111, C11S03, 2006.

Yang, Y., Shi, Y., Yu, C., Teng, Y., and Sun, M.: Study on surface wave-induced mixing of transport flux residue under
560   typhoon conditions, Journal of Oceanology and Limnology, 37, 1837-1845, https://doi.org/10.1007/s00343-019-8268-9, 2019.

Yang, Y., Zhan, R., and Teng, Y.: Parameterization of ocean wave-induced mixing processes for finite water depth, Acta Oceanologica Sinica, 28, 16-22, 2009.

Yu, C., Yang, Y., Yin, X., Sun, M., and Shi, Y.: Impact of Enhanced Wave-Induced Mixing on the Ocean Upper Mixed Layer during Typhoon Nepartak in a Regional Model of the Northwest Pacific Ocean, Remote Sensing, 12, 2808,
565   https://doi.org/10.3390/rs12172808, 2020.

Yu, W., Song, J., Cao, A., Yin, B., and Guan, S.: An Improved Second-Moment Closure Model for Langmuir Turbulence Conditions: Model Derivation and Validation, Journal of Geophysical Research Oceans, 123, 9010-9037, 2018.

Yuan, Y., Han, L., Qiao, F., Yang, Y., and Lu, M.: A unified linear theory of wavelike perturbations under general ocean conditions, Dynamics of Atmospheres and Oceans, 51, 55-74, https://doi.org/10.1016/j.dynatmoce.2010.11.001, 2011.

570   Yuan, Y., Hua, F., Pan, Z., and Sun, L.: LAGFD-WAM numerical wave model - I Basic physical model, Acta Oceanologica Sinica, 10, 483-488, 1991.

Yuan, Y., Hua, F., Pan, Z., and Sun, L.: LAGFD-WAM numerical wave model - II Characteristics inlaid scheme and its application, Acta Oceanologica Sinica, 11, 13-23, 1992.

Yuan, Y., Qiao, F., Yin, X., and Han, L.: Analytical estimation of mixing coefficient induced by surface wave-generated
575   turbulence based on the equilibrium solution of the second-order turbulence closure model, Science China Earth Sciences, 56, 71-80, 2013.

Zhao, Z.: Internal tide radiation from the Luzon Strait, Journal of Geophysical Research: Oceans, 119, 5434-5448, https://doi.org/10.1002/2014jc010014, 2014.

Zhao, Z.: The Global Mode-2 M2 Internal Tide, Journal of Geophysical Research: Oceans, 123, 7725-7746,
580   https://doi.org/10.1029/2018jc014475, 2018.

Zhao, Z., and Alford, M. H.: New Altimetric Estimates of Mode-1 M2 Internal Tides in the Central North Pacific Ocean, Journal of Physical Oceanography, 39, 1669-1684, https://doi.org/10.1175/2009jpo3922.1, 2009.

Zhao, Z., Alford, M. H., Girton, J. B., Rainville, L., and Simmons, H. L.: Global Observations of Open-Ocean Mode-1 M2 Internal Tides, Journal of Physical Oceanography, 46, 1657-1684, https://doi.org/10.1175/jpo-d-15-0105.1, 2016.

585 Zhuang, Z., Yuan, Y., and Yang, G.: An ocean circulation model in σS-z-σB hybrid coordinate and its validation, Ocean Dynamics, 68, 159-175, 2018.

Zhuang, Z., Zheng, Q., Yuan, Y., Yang, G., and Zhao, X.: A non-breaking-wave-generated turbulence mixing scheme for a global ocean general circulation model, Ocean Dynamics, 70, 293-305, 2020.